Journal of Neuroinflammation

RESEARCH Open Access

Dynamic phosphorylation of Fascin-1 orchestrates microglial phagocytosis and neurological recovery after spinal cord injury

Yanchang Liu[1,2†], Fei Yao[1,2†], Ziyu Li[1,2†], Yan Jiang[1,3], Jianjian Li[1,2], Shuisheng Yu[1,2], Xuyang Hu[1,2], Fangru Ouyang[1,2], Meige Zheng[1,2*], Li Cheng[1,2*] and Juehua Jing[1,2*]

Abstract

The persistence of myelin debris after spinal cord injury (SCI) constitutes a formidable barrier to axonal regeneration, remyelination, and functional recovery by initiating inflammatory cascades. Microglia, known for their superior phagocytic and degradative capabilities, are crucial in clearing myelin debris. Yet, the molecular mechanisms governing their function remain elusive. Our previous research has identified a sustained upregulation of Fascin-1, an actin-binding protein essential for phagocytosis, in Cx3cr1^{+} microglia after SCI. Here, we reveal that ablation of microglial Fascin-1 exacerbates neuronal loss and hampers motor recovery after SCI, correlating with diminished microglial phagocytic activity in *Cx3cr1*$^{cre+/-}$;*Fascin-1*$^{fl/fl}$ mice. We demonstrated that dysregulated Fascin-1 phosphorylation impairs microglial phagocytosis, linked to the upstream Mas1/Protein kinase C gamma (PKCγ) axis. Pharmacologic activation of the Mas1/PKC axis to drive Fascin-1 phosphorylation in microglia restores phagocytic function, thereby alleviating neuronal loss and facilitating neurological recovery after SCI. Our findings underscore the critical role of Fascin-1 phosphorylation in microglial phagocytosis and highlight the Mas1/PKCγ axis as a promising therapeutic target for SCI.

Introduction

Acute mechanical compression causing spinal cord injury (SCI) disrupts the integrity of myelin sheaths, leading to subsequent axonal demyelination and the generation of a significant amount of myelin debris [1]. As an external inhibitory factor at the injury site, myelin debris extensively mediates persistent inflammatory responses, axonal regeneration failure, fibrosis, and abnormal angiogenesis after SCI [2, 3]. Microglia, the immune surveillance cells of the central nervous system (CNS), act as the primary professional phagocytes responsible for clearing myelin debris from 24 h to 3 days post-injury (dpi) [4]. Additionally, microglia coordinate beneficial repair functions by interacting with astrocytes and infiltrating

†Yanchang Liu, Fei Yao and Ziyu Li contributed equally to this work.

*Correspondence:
Meige Zheng
zhengmg113@126.com
Li Cheng
chengli7788@163.com
Juehua Jing
jjhhu@sina.com
[1]Department of Orthopedics, The Second Affiliated Hospital of Anhui Medical University, Hefei, China
[2]Institute of Orthopedics, Research Center for Translational Medicine, The Second Affiliated Hospital of Anhui Medical University, Hefei, China
[3]Department of Rehabilitation Medicine, The Second Affiliated Hospital of Anhui Medical University, Hefei, China

monocyte-derived macrophages during the first week after SCI [5, 6]. However, the beneficial role of microglial phagocytosis diminishes as infiltrating macrophages increasingly supplant and inhibit this process, leading to the formation of foamy macrophages and exacerbation of inflammation by 7 dpi [4, 7]. Therefore, identifying novel and potent targets to enhance microglial phagocytosis represents a promising therapeutic strategy aimed at bolstering repair mechanisms following SCI.

Our previous study revealed that Fascin-1 is continuously upregulated and specifically expressed in microglia post-SCI [8]. Fascin-1, an intracellular actin-binding protein localized in the cytoplasm, plays a critical role in regulating the polymerization and stabilization of F-actin [9]. In another study, we initially investigated how Fascin-1 influences the mechanical properties in the microenvironment of SCI. Upregulated Fascin-1 may suppress the level of active myosin in microglia, decreasing the stiffness of the injured spinal cord [10]. Fascin-1 organizes F-actin into parallel bundles, while phosphorylation on Ser39 by protein kinase C (PKC) reduces its bundling ability, thereby priming the plasma membrane for deformation [11–13]. This process maintains F-actin in a dynamic state essential for cellular processes, including efficient phagocytosis by immune cells [14]. Based on these insights, we hypothesized that the dynamic phosphorylation of Fascin-1 mediates the clearance of myelin debris by microglia following SCI.

In this study, we demonstrated that microglial Fascin-1 deficiency impairs phagocytosis, exacerbating neuronal loss and worsening neurological recovery after SCI. Transcriptomic data analysis unveiled that Mas1 regulates Fascin-1 phosphorylation via PKCγ. Notably, we confirmed that targeting Fascin-1 activation through the Mas1 agonist captopril promotes microglial phagocytosis, facilitating axonal regeneration and neurological recovery after SCI. These results underscore the significance of the dynamic phosphorylation of Fascin-1, regulated by the Mas1/PKCγ axis, in orchestrating the clearance of myelin debris by microglia and improving neurological outcomes after SCI.

Materials and methods

Animals

All animal experiments were approved by the Institutional Animal Ethics Committee of Anhui Medical University (Approval No. LLSC20211113). All mice were in the C57BL/6J background. Wild type mice were purchased from the Experimental Animal Center of Anhui Medical University. *Cx3cr1*$^{cre+/-}$;*Fascin-1*$^{fl/fl}$ (*Fascin-1* CKO) mice were generated by crossbreeding *Cx3cr1*$^{cre+/-}$ (background C57BL/6J, Shanghai Model Organisms Center, Cat. NO. NM-KI-200079) and *Fascin-1*$^{fl/fl}$ (background C57BL/6J, Shanghai Model Organisms Center, Cat. NO. NM-CKO-210023). *Cx3cr1*$^{cre+/-}$ mice were a knock-in/knockout (KI/KO) strain, wherein the endogenous Cx3cr1 coding sequence was replaced by the Cre recombinase. Male and female mice were randomly assigned to different groups, ensuring a balanced distribution of sexes within each group. All mice were housed under specific pathogen-free conditions with suitable humidity and temperature. A 12-hour day-night cycle was maintained, and food and water were provided ad libitum.

Spinal cord crush injury model and drugs administration

The mice, aged 8–10 weeks, were anesthetized with intraperitoneal injection of sodium pentobarbital (50 mg/kg) and subjected to the standardized surgical protocols referring to our previous study [15]. Briefly, the mice underwent laminectomy at the thoracic eight vertebrae, followed by continuous crushing of the thoracic ten spinal cord for 5 s with No. 5 Dumont forceps (Fine Science Tools, CA), resulting in a distinct clamp mark. The injured mice were then resuscitated in an incubator (22–24 °C) until full awake. All mice received a daily subcutaneous injection of Baytril (10 mg/kg) for anti-infection for 1 week, and bladder care was supplied twice daily to prevent urinary retention. Mice that experienced a weight loss greater than 25% within the 3 dpi, mice with significant post-operative swelling in the hind limbs, and mice with infection at the surgical site were excluded from the functional motor assessments.

The mice in the captopril treatment group were daily intraperitoneally injected with captopril (39 mg/kg, S2051, Selleck, United States), an agonist of the ACE2/Ang-(1–7)/Mas1 axis, after injury until 28 dpi. The mice in the control group received intraperitoneal injection of equivalent volume of control solvent saline.

Tissue Preparation

For western blot analysis, the mice underwent transcardial perfusion with cold phosphate-buffered saline (PBS, BL601A, Biosharp, China). Subsequently, a spinal cord segment (0.3 cm length) spanning the lesion core was dissected. For immunofluorescence staining, the mice were transcardially perfused with PBS and then perfused with 4% paraformaldehyde (PFA, G1101, Servicebio, China). The dissected spinal cord segment (0.5 cm length) spanning the lesion core was then subjected to programmed post-fixation, dehydration and paraffin embedding. Finally, serial 6 μm thick sagittal sections encompassing the lesion core were obtained using a microtome (RM2235, Leica, Germany).

Preparation and administration of Myelin debris

The brain tissue from mixed sex mice aged 6–8 weeks was harvested and homogenized in 0.32 M sucrose

solution on ice. Myelin debris were isolated via sucrose density gradient centrifugation, as previously described [16]. Subsequently, the myelin debris were mixed with 3,3'-Dioctadecyloxacarbocyanine perchlorate (DIO, C1993S, Beyotime, China) and incubated at 37 °C for 20 min in the dark. In all in vitro experiments, DIO-labeled myelin debris were added into cells at a final concentration of 1 mg/ml.

Primary microglia extraction, culture, and intervention

Neonatal mice (postnatal days 1 to 4) of mixed sex were euthanized for the extraction of primary microglia following the previously described protocol [17]. After removing the olfactory bulb and cerebellum, the brains were minced in ice-cold PBS and collected in 6-well plates. The brain tissue was incubated with 0.5 ml digestion buffer per brain (C0203, Beyotime, China) in a 5% CO_2, 37 °C incubator for 20 min. Then, a 40 μm cell strainer was used to filter the resulting single-cell suspension, followed by centrifugation at 200 g for 10 min at room temperature. After resuspension in 5 ml DMEM (12100046, Gibco, United States), the cells were seed at a density of approximately 5×10^6 in T25 or T75 flasks and cultured in a 5% CO_2, 37 °C incubator. After 4 days, the flasks were shaken at 180 rpm for 30 min on an incubator shaker. Microglia can be harvested for up to one month thereafter. Collect the culture medium from the LADMAC cells (CRL-2420, ATCC, United States), centrifuge at 200 x g for 10 min, filter using 0.22 μm cell strainer to prepare 20% LADMAC conditioned medium. The primary microglia were cultured in DMEM medium containing 20% LADMAC medium, 10% fetal bovine serum (FBS, 10270106, Gibco, United States), and 1% penicillin-streptomycin (C0222, Beyotime, China) in a 5% CO2, 37 °C incubator [17].

For PKC activating or blocking experiments, microglia were pretreated with either the agonist 12-O-tetradecanoylphorbol 13-acetate (TPA, 10 ng/ml, S7791, Selleck, United States) or the inhibitor Bisindolylmaleimide I (BIM, 25 μg/ml, S7208, Selleck, United States) for 12 h. Subsequently, microglia were treated with myelin debris for 6 h. For the day 5-treated microglia, they had been exposed to myelin debris for 5 days prior. Then, For knockdown of *Fascin-1* gene in vitro, a siRNA targeting mouse *Fascin-1* (siRNA: 5'-GAUCCAACCGUUCCAG UUTT-3') and a nonspecific control siRNA (NC: 5'-GC CTTCAUGAACTAATCTU-3') were purchased from GenePharma (Shanghai, China). These siRNAs were transfected into microglia using jetPRIME (114 – 15, Polyplus, United States) according to the manufacturer's instructions.

Transcriptomic dataset analysis

Based on the Gene Expression Omnibus (GEO) database (https://www.ncbi.nlm.nih.gov/geo/), we obtained all differentially expressed genes of injury-activated microglia/ macrophages (GSE113566). The Metascape (https://metascape.org/) was used to perform Gene Ontology (GO) enrichment analysis focusing on biological processes. The differentially expressed genes were uploaded to the Metascape with parameters set to P Value Cutoff = 0.05 and Min Enrichment = 0.3. Following completion of the enrichment analysis, the dataset was exported and sorted based on the Enrichment value. The top 10 GO enrichment results were then illustrated. The search terms "G protein coupled receptors family" or "protein kinase C family" were used to search for target genes and the results were presented using GraphPad Prism 8.0 (GraphPad, United States).

Immunofluorescence staining

For tissue immunofluorescence staining, the 6 μm thick spinal cord sections spanning the lesion core were subjected to the staining procedure as previously described [18]. Briefly, the sections were blocked in PBS buffer containing 10% donkey serum albumin (DSA, SL050, Solarbio, China) and 0.3% Triton X-100 (T8200, Solarbio, China) at room temperature for 1 h. Then, the sections were incubated with primary antibodies at 4 °C overnight, followed by incubation with corresponding secondary antibodies at room temperature for 1 h. The primary antibodies utilized were as follows: mouse anti-Fascin-1 antibody (1:50, sc-21743, Santa Cruz, United States), rabbit anti-p-Fascin-1 antibody (1:100, ab90618, Abcam, United States), mouse anti-Mas1 antibody (1:50, sc-390453, Santa Cruz, United States), rabbit anti-Cx3cr1 antibody (1:100, ab8021, Abcam, United States), mouse anti-Cx3cr1 antibody (1:50, sc-377227, Santa Cruz, United States), rat anti-GFAP antibody (1:100, 13–0300, Invitrogen, United States), rabbit anti-NeuN antibody (1:100, 24307, CST, United States), rabbit anti-MBP antibody (1:100, AB5864, Merck, Germany), mouse anti-PKCα antibody (1:50, sc-8393, Santa Cruz, United States). The secondary antibodies used were Alexa Fluor 488 and Alexa Fluor 555 (1:500, A-2206, A-2202, A-2203, A-21207, and A11058, Invitrogen, United States). Nuclei were stained with 4',6-diamino-2-phenylindole (DAPI, P0126, Beyotime, China). The immunofluorescence images were acquired using Axio Scope A1 microscope and LSM 900 microscope (Zeiss, Germany). Quantitative analysis was performed using ImageJ 2.0 (NIH, United States).

For cell immunofluorescence staining, cells were fixed with 4% PFA for 15 min, permeabilized with 0.5% Triton X-100 in PBS for 10 min, and then blocked with 10% DSA in PBS for 30 min at room temperature. Primary

antibodies (as listed above) were diluted with 1% DSA in PBS and incubated overnight at 4 °C. Secondary antibodies (as listed above) were diluted with 1% DSA in PBS and incubated for 1 h at room temperature. Phalloidin (1:200, C2203S, Beyotime, China) specifically bound to F-actin (red fluorescence) was used to identify the cellular morphology and contour.

Luxol fast blue staining

The steps were conducted following the manufacturer's instructions (Luxol fast blue staining kit, C0631S, Beyotime, China). The Luxol fast blue (LFB) staining solution was preheated at 60 °C for 30 min. The sections were then immersed in LFB staining solution for 2 h at 60 °C. After rinsing in distilled water, the sections were immersed in differentiation solution for 15 s and 70% ethanol for 30 s. Light microscopy was used to examine LFB-stained tissue sections for the analysis of myelin preservation.

Western blot

The total spinal cord protein was extracted with RIPA buffer (R0278, Sigma, United States) supplemented with a protease inhibitor (04693124001, Roche, Switzerland) and a phosphatase inhibitor (04906845001, Roche, Switzerland). The extracted protein was quantified with BCA protein detection kit (P0010S, Beyotime, China). 20 μg of protein per sample was resolved on SDS-PAGE electrophoresis and transferred onto a polyvinylidene difluoride (PVDF) membrane. The PVDF membranes were blocked with 5% nonfat milk in TBST (ST671, Beyotime, China) and then incubated in the primary antibody at 4 °C overnight. The corresponding secondary antibody was incubated at room temperature. All antibodies were dissolved in antibody diluent (P0268, Beyotime, China). The primary antibodies included mouse anti-Fascin-1 (1:1000, sc-21743, Santa Cruz, United States), rabbit anti-p-Fascin-1 (1:1000, ab90618, Abcam, United States), mouse anti-Mas1 (1:1000, sc-390453, Santa Cruz, United States), rabbit anti-PKCγ (1:1000, 14364-1-AP, Proteintech, China), rabbit anti-PKCγ (phospho T655) (1:1000, ab5796, Abcam, United States), mouse anti-PKCα (1:1000, sc-8393, Santa Cruz, United States), mouse anti-GAPDH (1:2000, 60004-1-Ig, Proteintech, China). To avoid interference, the blots for Fascin-1 and p-Fascin-1, PKCα and PKCγ antibody incubations were obtained from separate PVDF membranes, rather than from elution of the same membrane. GAPDH was probed on each gel alongside target proteins. The HRP-conjugated secondary antibodies included goat anti-mouse antibody (1:100000, A4416, Sigma, United States) and goat anti-rabbit antibody (1:100000, A0545, Sigma, United States). The protein band was detected with ECL detection kit (35055, Thermo Fisher Scientific, United States) and Tanon 5200 system (Tanon, China). The gray values of specific bands were analyzed by normalizing their levels to each GAPDH. Each group involved three individual mice or three independent cultures in the experiment. ImageJ 2.0 was used for quantitative analysis.

Image acquisition and quantitative analysis

All the representative images were obtained by a Zeiss LSM 900 confocal microscope system and a Zeiss Axio Scope A1 fluorescence microscope. Post-processing of these images was conducted using ZEN 3.3 software and ImageJ 2.0 software.

For immunostained Z-stack images in vivo, a z-step of 1.5 μm was used to acquire the confocal images, resulting in 12–13 sections per stack. To quantify $Cx3cr1^+$/MBP^+ cells, the nucleus of the cell of interest was defined. Positive co-localization staining was determined in 6 randomly picked areas and calculated the proportion of $Cx3cr1^+$/MBP^+ cells. To quantify $Cx3cr1^+$, $Mas1^+$, $Fascin\text{-}1^+$ and $p\text{-}Fascin\text{-}1^+$ cells in vivo, a 100 μm square grid spanning the lesion core was generated. Targeted cells with $DAPI^+$ staining were quantified in every 6th square. To quantify the number of residual $NeuN^+$ neurons around the lesion core, sections were divided into three zones based on distance from the lesion core: Z1 (0–250 μm), Z2 (250–500 μm), Z3 (500–750 μm) and Z4 (750–1000 μm) calculated the number of positive stained cells for each region as described previously [19, 20]. Microglia exhibiting phagocytic activity were defined as $Cx3cr1^+$ cells containing distinct MBP^+-stained myelin debris. The phagocytic capacity was quantified as the ratio of $Cx3cr1^+$/MBP^+ cells to the total $Cx3cr1^+$ population.

For immunofluorescence images in vitro, a total of > 10 randomly selected cells in each slide were processed to obtaining mean fluorescence intensity of PKCα, PKCγ, Fascin-1, p-Fascin-1 and Mas1. To quantify microglial phagocytosis, 10 randomly selected cells were collected and measured the fluorescence intensity of Dio-myelin per $Phalloidin^+$ cell. 3 independent cultures in vitro were selected. All quantitative analyses were performed blindly.

Motor function assessments

The Basso Mouse Scale (BMS) score was used to assess motor function of mice at 0, 1, 3, 7, 14 and 28 dpi, with 7 animals per group. Scores range from 0 to 9, with 0 representing complete paralysis and 9 representing normal motor function. The final score for each mouse was calculated as the average of the assessments conducted by two blinded researchers.

Footprint analysis was employed to further evaluate motor function recovery at 28 dpi. Fore and hind paws of each mouse were stained with green and red dyes, respectively. The stride length was determined by the

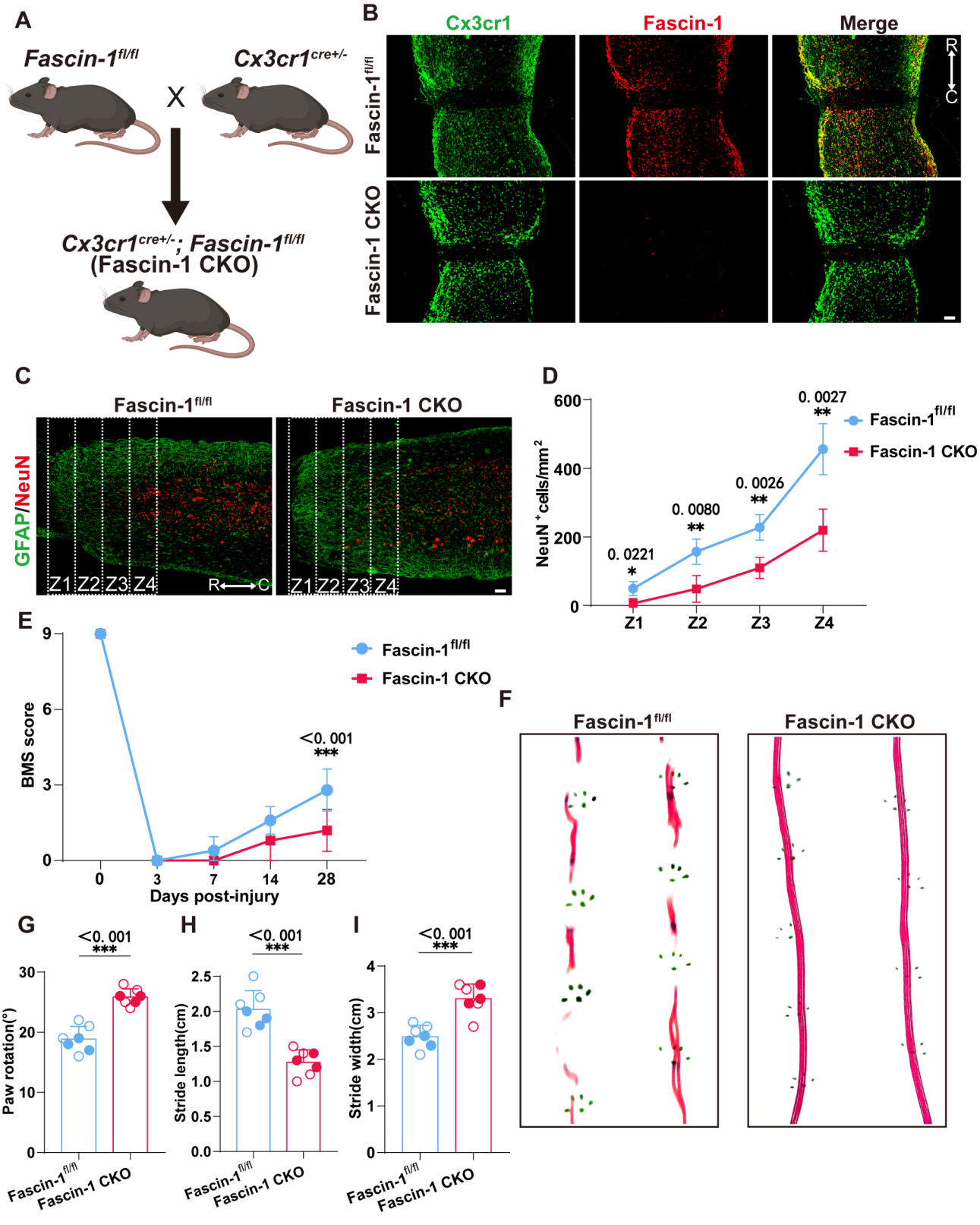

Fig. 1 (See legend on next page.)

(See figure on previous page.)

Fig. 1 Ablation of Fascin-1 in microglia exacerbates neuronal loss and inhibits motor recovery after SCI. (**A**) Pattern diagram of the construction of *Cx3cr1*$^{cre+/-}$;*Fascin-1*$^{fl/fl}$ (Fascin-1 CKO) mice. (**B**) Immunofluorescent staining verified the knockdown efficiency of Fascin-1 (red) in Cx3cr1^{+} microglia (green) at 14 dpi. R and C represent the rostral and caudal sides of the injury, respectively. (**C**) Representative immunofluorescence images of GFAP^{+} astrocytes (green) and NeuN^{+} neurons (red) in Z1-Z4 zones adjacent to the lesion core in mice at 28 dpi. (**D**) Quantification of NeuN^{+} neurons in (**C**). (**E**) Behavioral testing using the BMS score was performed at 0–28 dpi. $^{*}p < 0.05$, $^{***}p < 0.001$ in (**D**) and (**E**) by twoway ANOVA followed by Tukey's post hoc test. (**F**) Footprint assays in *Fascin-1*$^{fl/fl}$ and *Fascin-1* CKO mice at 28 dpi. (**G**-**I**) Quantification of Paw rotation (**G**), Stride length (**H**), and Stride width (**I**) in Footprint assays (**F**). Hollow data points represent values from male mice. Solid data points denote female mice. Scale bars: 100 μm (**B**) and (**C**). R and C represent the rostral and caudal sides of the injury respectively. Data are presented as means ± SD. $n = 7$ mice per group in (**D**), (**E**) and (**G**-**I**). $^{***}p < 0.001$ in (**G**-**I**) by Student's t test

distance of the hind paws from start to finish in a step. The stride width was determined by the distance between the most lateral toes of the left and right paws. The rotation of the paw was determined by the angle between the body midline axis and the axis of the hind paw. All assessments were performed over three consecutive gait cycles per side, with 7 animals per group. All evaluations were performed blindly.

Statistical analysis

The data were presented as mean ± standard deviation (SD). In all the bar charts, each data point represents an individual animal or an independent culture. Hollow data points represent values from male mice and solid data points denote female mice. One-way or two-way analysis of variance (ANOVA) followed by Tukey's post hoc test was used for comparisons among multiple groups. Student's t test was used for comparisons between two groups. Data analysis and graphing were performed with GraphPad Prism 8.0. $p < 0.05$ was considered statistically significant.

Results

Microglial Fascin-1 knockout exacerbates neuronal loss and impairs locomotor function recovery after SCI

Building upon our prior findings that Fascin-1 is consistently and specifically upregulated in Cx3cr1^{+} microglia after SCI, we constructed conditional Fascin-1 knockout in microglia (*Cx3cr1*$^{cre+/-}$;*Fascin-1*$^{fl/fl}$, *Fascin-1* CKO) mice to further explore the function of Fascin-1 in microglia after SCI (Fig. 1A) [8]. Immunofluorescence staining confirmed the targeted ablation of Fascin-1 in microglia, with rare expression of Fascin-1 at 14 dpi (Fig. 1B; Supplemental Fig. 1A). To evaluate neuronal survival, we selected 4 designated regions (Z1-Z4) from the rostral to caudal end and measured the number of NeuN^{+} cells/mm^{2} in each portion [19, 20]. *Fascin-1* CKO mice displayed a marked reduction in residual NeuN^{+} neurons within the Z1-Z4 regions compared to their *Fascin-1*$^{fl/fl}$ counterparts (Fig. 1C and D). *Fascin-1* CKO mice showed a significantly decreased LFB^{+} area compared with *Fascin-1*$^{fl/fl}$ mice at 28 dpi (Supplemental Fig. 2A and 2B). Additionally, the BMS scores of *Fascin-1* CKO mice were significantly lower at 28 dpi (Fig. 1E), and footprint analysis revealed worse locomotor function characterized by hind paws dragging, longer step widths, and greater paw rotations (Figs. 1F-I). These results indicate that Fascin-1 is pivotal for microglial neuroprotective function in mitigating neuronal loss and facilitating locomotor function recovery after SCI.

Fascin-1 modulates microglial phagocytosis of Myelin debris after SCI

Microglia are rapidly activated to phagocytize and degrade myelin debris during the acute phase of SCI, which aids in resolving inflammation and preserving neurons [21, 22]. To uncover the role of Fascin-1 in microglial phagocytosis, we detected the changes in microglial phagocytosis of MBP^{+} myelin debris in the injured *Fascin-1* CKO mice. Immunofluorescence results showed that microglial phagocytosis of myelin debris, represented by Cx3cr1^{+}MBP^{+} microglia, was mainly observed in the acute phase of SCI (1 and 3 dpi), while *Fascin-1* CKO mice exhibited a lower proportion of Cx3cr1^{+}MBP^{+} microglia at 1, 3, and 7 dpi compared to *Fascin-1*$^{fl/fl}$ mice (Figs. 2A and 2B). Compared to the Wild type (WT) group, *Cx3cr1*$^{cre+/-}$ mice exhibited a 30% reduction in the phagocytic capacity of WT microglia. Meanwhile, *Fascin-1 CKO* mice exhibited nearly a 60% loss of this capacity than *Cx3cr1*$^{cre+/-}$ control (Supplemental Figs. 3A and 3B). This suggests that Fascin-1 knockout in microglia impedes their phagocytosis of myelin debris after SCI. To corroborate these in vivo findings, we established an in vitro primary microglia culture system. A siRNA targeting Fascin-1 was transfected to knockdown Fascin-1 in microglia, Dio-myelin debris was added 24 h later. The co-localization of phalloidin-labeled microglia with Dio-myelin showed that microglial phagocytosis of myelin debris increased until 3 days after induction but was decreased by more than 50% at 5 days (Figs. 2C and 2D), consistent with the in vivo findings that microglia exhibited robust phagocytic capacity during the acute phase (1–3 dpi) but experienced phagocytosis blockade at 7 dpi (Figs. 2A and 2B). Importantly, low co-localization levels of microglia and Dio-myelin during 0–5 d (< 10% in Myelin + siFascin-1 group) indicated that targeted knockdown of Fascin-1 in microglia significantly impaired their phagocytosis of myelin debris (Figs. 2C and 2D; Supplemental Figs. 1B and 1C). These results suggest that

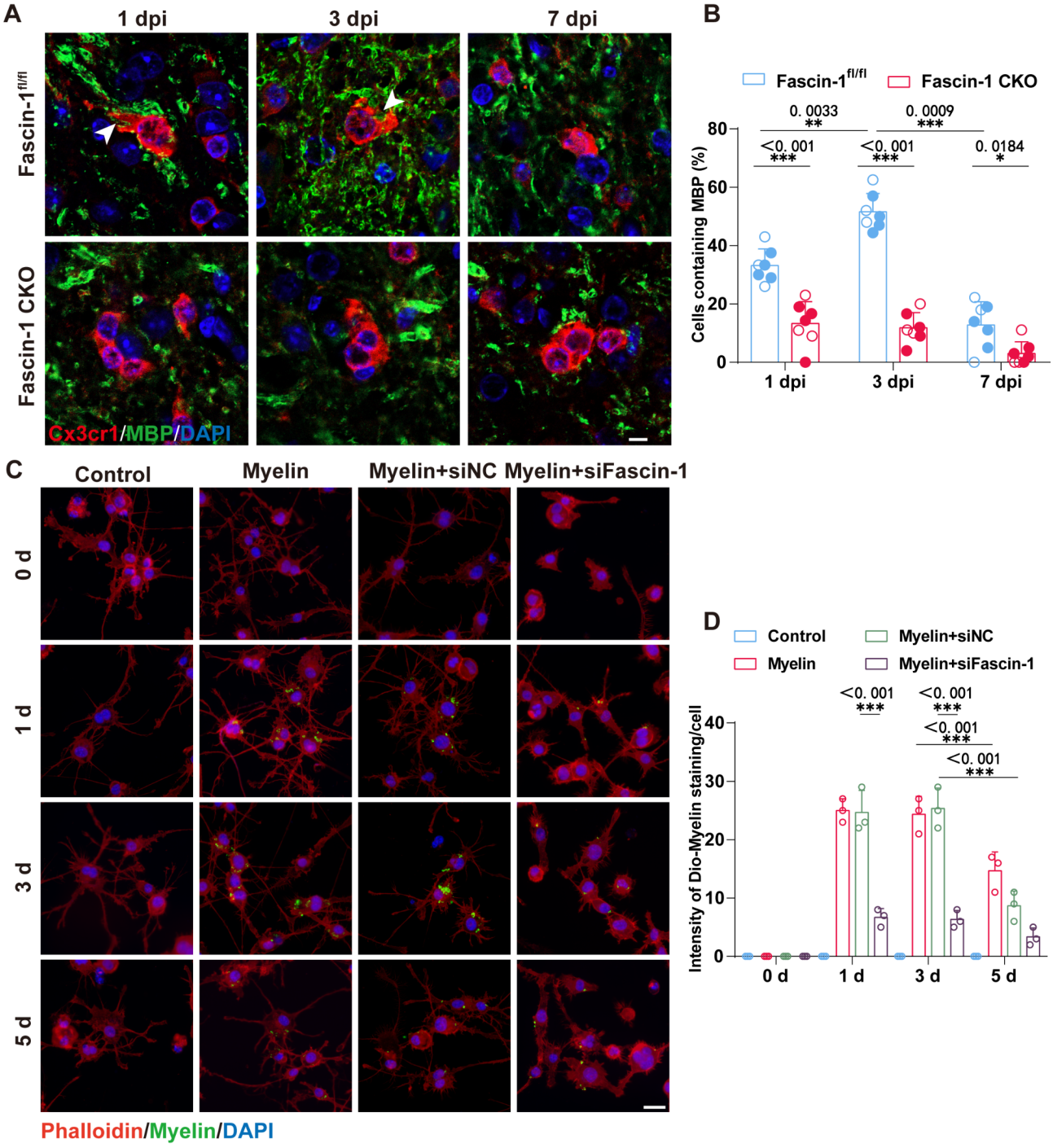

Fig. 2 Fascin-1 regulates microglial phagocytosis in vivo and vitro (**A**) Representative immunofluorescence images of Cx3cr1^{+} microglia (red) and MBP (green) at 1, 3 and 7 dpi in *Fascin-1*$^{fl/fl}$ and *Fascin-1* CKO mice. White arrowheads indicate microglia phagocytosing MBP. (**B**) Quantification of the percentage of Cx3cr1^{+} cells containing MBP in (**A**). Hollow data points represent values from male mice. Solid data points denote female mice. (**C**) Representative immunofluorescence images of primary microglia (phalloidin staining, red) incubated with Dio-myelin (1 mg/ml, green) at 0–5 d in vitro. (**D**) Quantification of intensity of Dio-Myelin staining/cell in (**C**). Scale bars: 5 μm (**A**) and 20 μm (**C**). Data are presented as means ± SD. $n = 7$ mice per group in (**B**). $n = 3$ independent cultures in (**D**). $^{*}p < 0.05$, $^{**}p < 0.01$, $^{***}p < 0.001$ by twoway ANOVA followed by Tukey's post hoc test

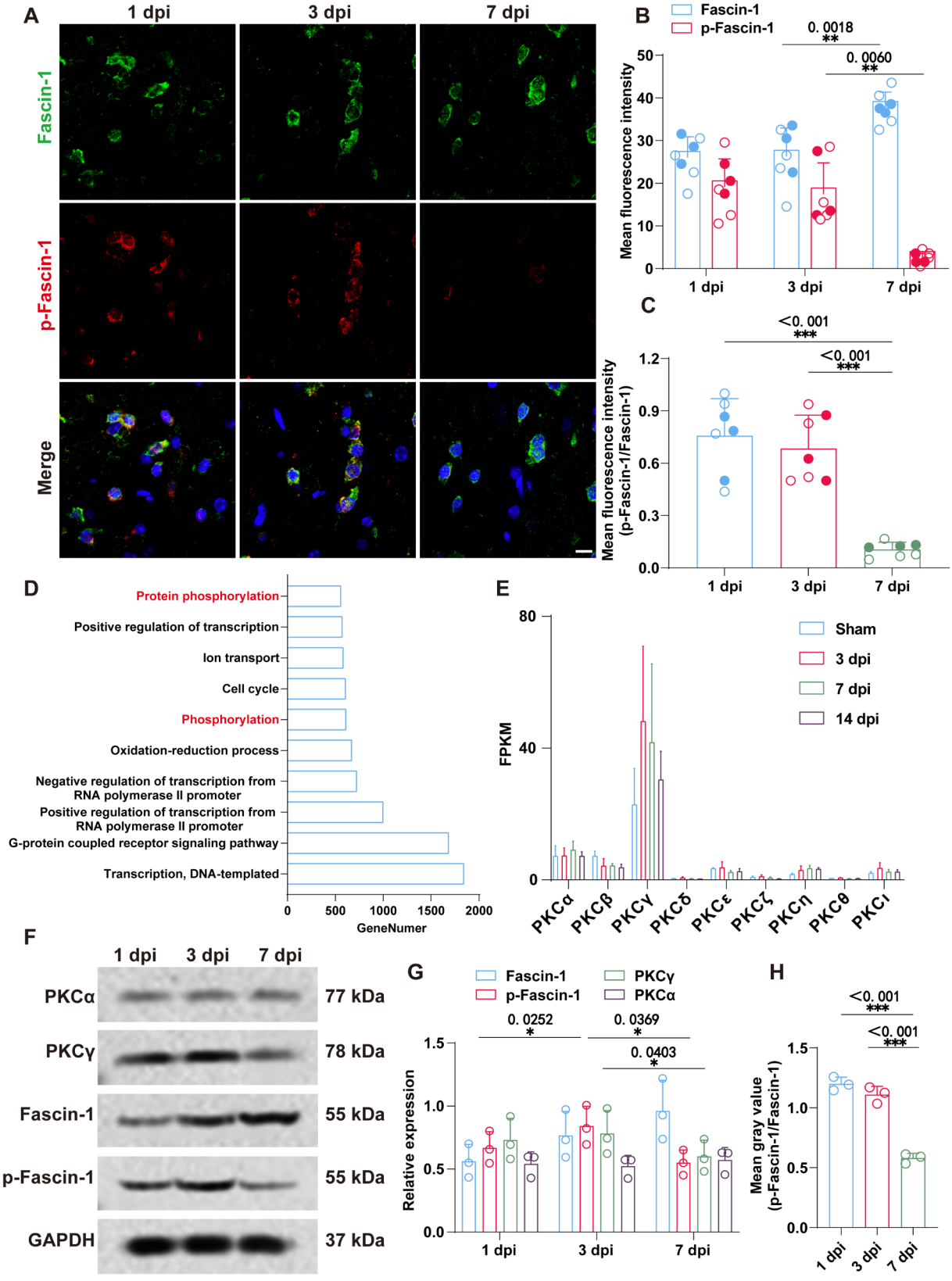

Fig. 3 (See legend on next page.)

(See figure on previous page.)

Fig. 3 Impaired microglial phagocytosis is accompanied by downregulation of Fascin-1 phosphorylation in vivo (**A**) Representative immunofluorescence images of p-Fascin-1 (red) and Fascin-1 (green) at 1, 3, and 7 dpi in WT mice. (**B**) Quantification of Mean Fluorescent Intensity (MFI) for p-Fascin-1 and Fascin-1 at 1, 3, and 7 dpi in WT mice. Hollow data points represent values from male mice. Solid data points denote female mice. (**C**) Quantification of p-Fascin-1/Fascin-1 in (**A**). (**D**) Gene ontology (GO) analysis of the published transcriptomic data (GSE113566) depicts the top 10 functional categories of differentially expressed genes in macrophages/microglia after SCI. (**E**) Bar graph of the average expression levels of PKC family members at 0–14 dpi in macrophages/microglia. (**F**) Western blot analysis of Fascin-1, p-Fascin-1, PKCα and PKCγ at 1, 3, and 7 dpi in WT mice. (**G**) Quantification of Fascin-1, p-Fascin-1, PKCα and PKCγ at 1, 3, and 7 dpi in WT mice (relative to GAPDH expression) in (**F**). (**H**) Quantification of p-Fascin-1/Fascin-1 in (**F**). Scale bar: 10 μm (**A**). Data are presented as means ± SD. $n = 7$ mice per group in (**B**) and (**C**). $n = 3$ mice per group in (**G**) and (**H**). $^{*}p < 0.05$, $^{**}p < 0.01$ by oneway ANOVA followed by Tukey's post hoc test

Fascin-1 is essential for microglial phagocytosis of myelin debris after SCI.

Fascin-1 phosphorylation is key to enhancing microglial phagocytosis

The dynamic balance between Fascin-1 phosphorylation and dephosphorylation is critical for maintaining plasma membrane deformation, thereby modulating phagocytosis and migration [9]. To explore whether Fascin-1 phosphorylation modulates microglial phagocytosis, we assessed the expression levels of Fascin-1 and phosphorylated Fascin-1 (p-Fascin-1) in vivo between 1 and 7 dpi. Immunofluorescence results showed that comparable expression levels of p-Fascin-1 and Fascin-1 at 1 and 3 dpi in SCI mice, corresponding to the period of robust microglial phagocytosis (Figs. 3A-C). However, the p-Fascin-1/Fascin-1 ratio decreased by 60–70% at 7 dpi, coinciding with reduced microglial phagocytic activity (Figs. 3A-C). Western blot analysis corroborated that Fascin-1 phosphorylation levels were similar at 1 and 3 dpi but decreased by nearly 50% at 7 dpi, aligning with the immunofluorescence results (Figs. 3F-H). This indicates a positive correlation between Fascin-1 phosphorylation and microglial phagocytic activity.

Fascin-1 phosphorylation is primarily driven by the PKC family [11, 12, 23]. To elucidate the hypothesis that PKC triggers Fascin-1 phosphorylation and mediates microglial phagocytosis, we analyzed the published transcriptomic data (GSE113566) of macrophages/microglia after SCI [24]. The GO/KEGG analysis showed that phosphorylation was a key enrichment criterion for differentially expressed genes (DEGs) within 7 dpi (Fig. 3D). Further analysis of PKC subtype expression in macrophages/microglia for 14 dpi revealed higher levels of PKCα and PKCγ, with PKCγ exhibiting more pronounced changes (Fig. 3E). Western blot results indicated that the expression level of PKCγ peaked at 3 dpi but significantly decreased at 7 dpi, while PKCα expression remained unchanged from 1 to 7 dpi (Figs. 3F-H). We further verified these findings in an in vitro microglia culture system with myelin debris induction. Immunofluorescence results showed significantly higher PKCγ expression compared to PKCα during the period of robust microglial phagocytosis at 1 and 3 days after induction, but the expression of PKCγ was decreased by nearly 50% at 5 days (Figs. 4A and 4B). Immunofluorescence and western blot results further confirmed that p-Fascin-1/Fascin-1 ratio and PKCγ expression were upregulated at 1 and 3 days but significantly downregulated at 5 days post-induction (Figs. 4C-G). These results suggest that the balance of Fascin-1 phosphorylation, particularly the elevation of p-Fascin-1/Fascin-1 ratio, contributes to microglial phagocytosis, with PKCγ as a major kinase for Fascin-1 phosphorylation.

Targeting PKCγ activation promotes Fascin-1 phosphorylation and enhances microglial phagocytosis

Considering the decreased phagocytosis of myelin debris by microglia at 5 d, accompanied by a significant decrease in p-Fascin-1 and PKCγ, we administered the TPA to activate the PKCγ pathway in primary microglia at days 0 and 5 in vitro to explore the role of PKCγ in Fascin-1 phosphorylation and microglial phagocytosis. At 5 days after myelin debris induction, immunofluorescence results showed that TPA efficiently activated the phosphorylation of Fascin-1, accompanied by the enhancement of microglial engulfment of myelin debris (Figs. 5A, 5C, 5D and 5E). Western blot showed that the expression of p-Fascin-1 and p-PKCγ was significantly increased at 5 days after myelin debris induction in vitro, further suggesting that PKCγ activated by TPA in microglia promoted Fascin-1 phosphorylation (Figs. 5A, 5B, 5F, 5G and 5H). These findings indicate that targeting PKCγ activation can promote Fascin-1 phosphorylation and rescue microglial phagocytosis blockade.

Mas1 is an upstream signaling molecule in the PKC/Fascin-1 pathway regulating microglial phagocytosis

G protein-coupled receptors are well-established upstream signaling molecules that activate various PKC subtypes [25, 26]. To further explore the upstream regulatory molecules of PKCγ that mediate Fascin-1 phosphorylation, we analyzed the transcriptomic data of macrophages/microglia after SCI, focusing on G protein-coupled receptors [24]. The data revealed that Mas1 exhibited the highest fold change among 24 examined G protein-coupled receptors at 3 dpi (Figs. 6A). Immunofluorescence staining of the injured spinal cord showed that Mas1 was highly colocalized with $Cx3cr1^{+}$ microglia, with $Cx3cr1^{+}Mas1^{+}$ microglia accounting for up to

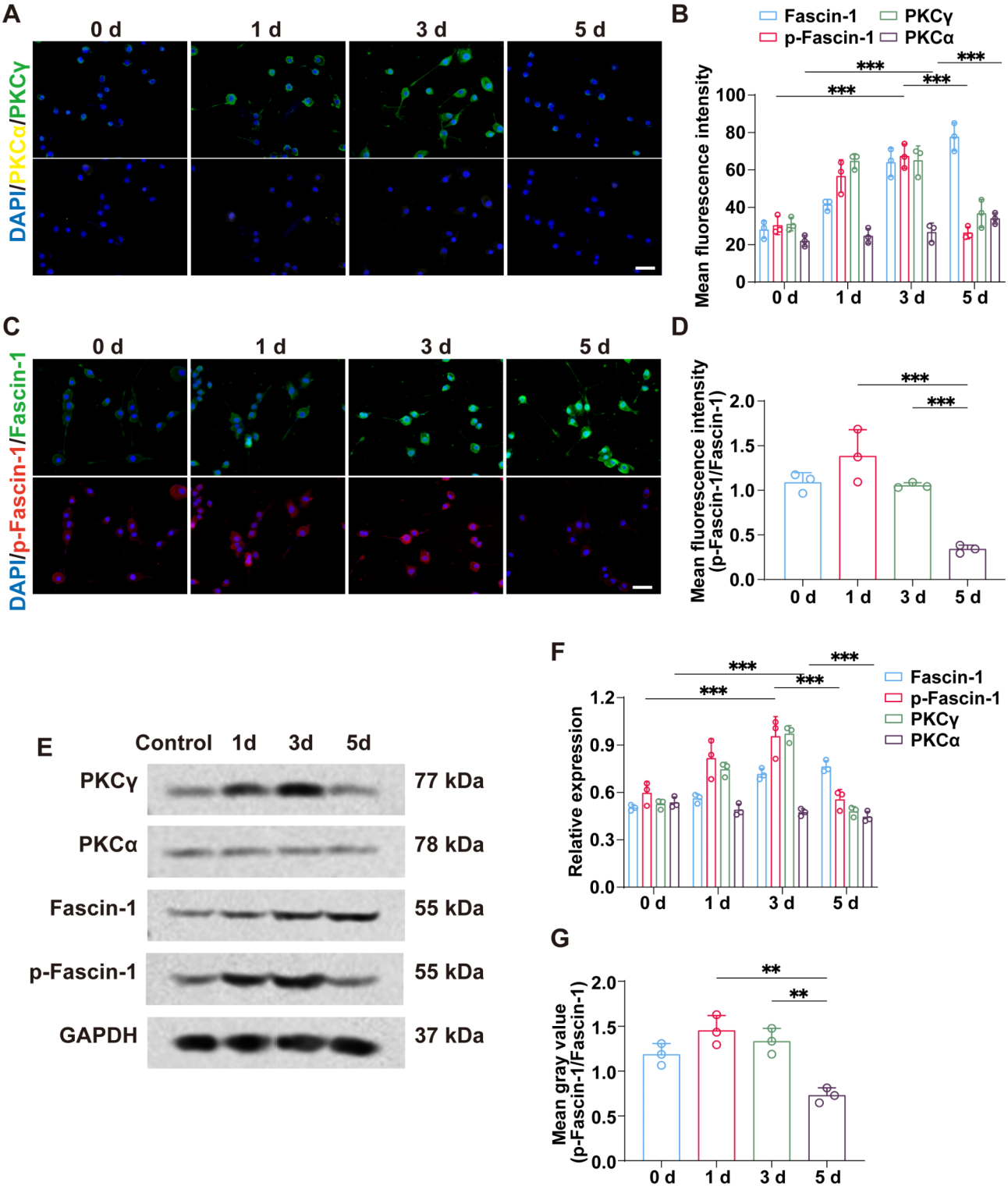

Fig. 4 The change trend of Fascin-1 phosphorylation during microglial phagocytosis in vitro. (**A**) Representative immunofluorescence images of PKCα (red) and PKCγ (green) in primary microglia incubated with myelin (1 mg/ml) at 0–5 d. (**B**) Quantification of MFI for Fascin-1, p-Fascin-1, PKCα and PKCγ at 0–5 d. (**C**) Representative immunofluorescence images of p-Fascin-1 (red) and Fascin-1 (green) in primary microglia incubated with myelin (1 mg/ml) at 0–5 d. (**D**) Quantification of p-Fascin-1/Fascin-1 in (**C**). (**E**) Western blot analysis of Fascin-1, p-Fascin-1, PKCα and PKCγ in primary microglia incubated with myelin (1 mg/ml) at 0–5 d. (**F**) Quantification of Fascin-1, p-Fascin-1, PKCα and PKCγ at 0–5 d (relative to GAPDH expression) in (**E**). (**G**) Quantification of p-Fascin-1/Fascin-1 in (**E**). Scale bars: 20 μm (**A**) and (**C**). Data are presented as means ± SD. $n = 3$ independent cultures in (**B**), (**D**), (**F**), and (**G**). $^{*}p < 0.05$, $^{**}p < 0.01$, $^{***}p < 0.001$ by oneway ANOVA followed by Tukey's post hoc test

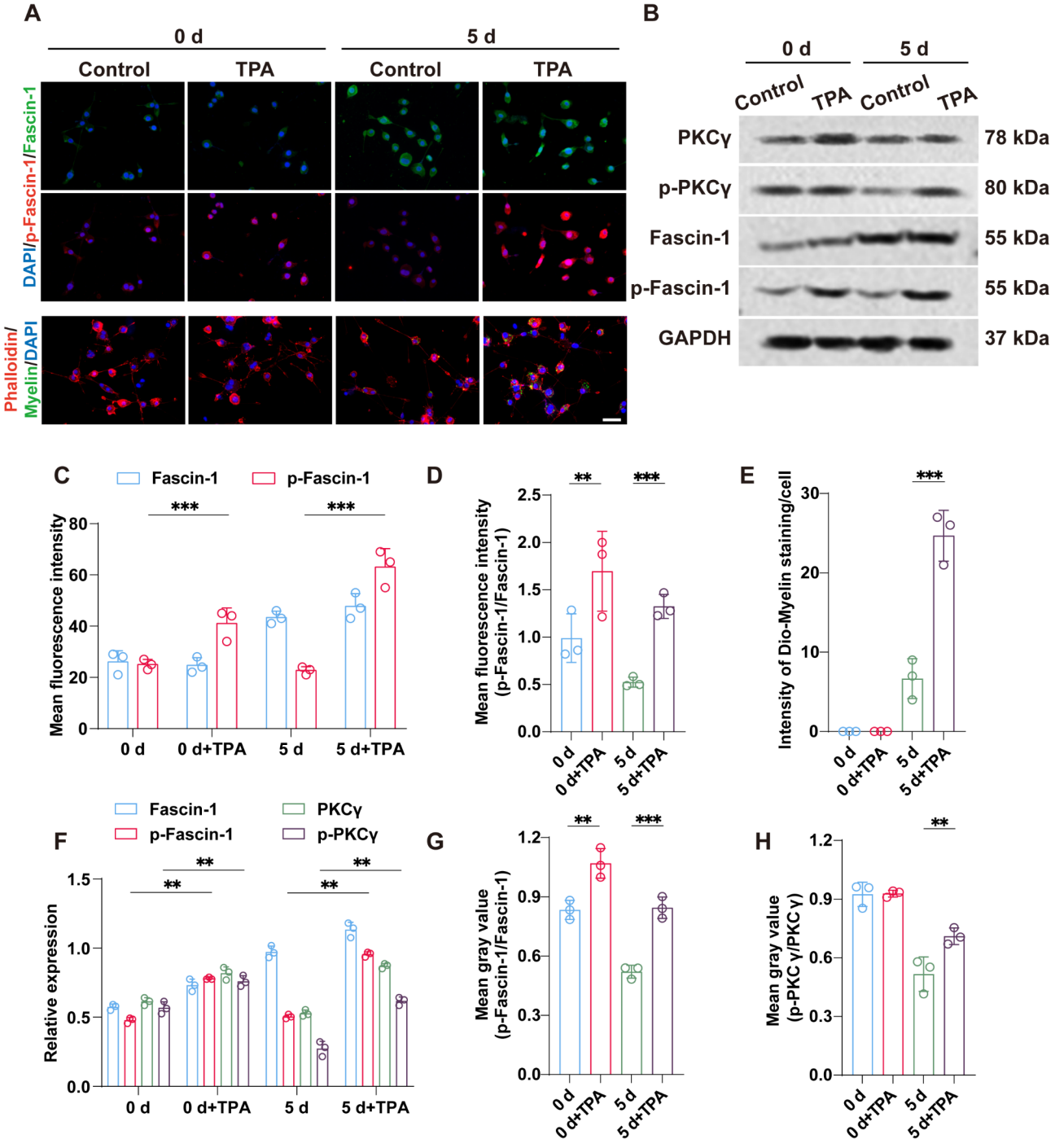

Fig. 5 Upregulation of Fascin-1 phosphorylation partially restores microglial phagocytosis in primary microglia in vitro. (**A**) Representative immunocytochemistry images of p-Fascin-1 (red), Fascin-1 (green) and primary microglia (phalloidin staining, red) incubated with Dio-myelin (1 mg/ml, green) at 0 or 5 d in primary microglia treated with or without TPA (10 ng/ml, an agonist of PKCγ). (**B**) Western blot analysis of Fascin-1, p-Fascin-1, PKCγ and p-PKCγ in primary microglia incubated with myelin (1 mg/ml) at 0 or 5 d treated with or without TPA (10 ng/ml). (**C**) Quantification of MFI for p-Fascin-1, Fascin-1 at 0 or 5 d in primary microglia treated with or without TPA (10 ng/ml) in (**A**). (**D**) Quantification of p-Fascin-1/ Fascin-1 in (**A**). (**E**) Quantification of intensity of Dio-Myelin staining/cell in (**A**). (**F**) Quantification of Fascin-1, p-Fascin-1, PKCγ and p-PKCγ in primary microglia incubated with myelin (1 mg/ml) at 0 or 5 d treated with or without TPA (10 ng/ml) (relative to GAPDH expression) in (**B**). (**G**) Quantification of p-Fascin-1/Fascin-1 in (**B**). (**H**) Quantification of p-PKCγ/PKCγ in (**B**). Scale bar: 20 μm (**A**). Data are presented as means ± SD. $n = 3$ independent cultures in (**B**-**H**). $^{*}p < 0.05$, $^{**}p < 0.01$, $^{***}p < 0.001$ by oneway ANOVA followed by Tukey's post hoc test

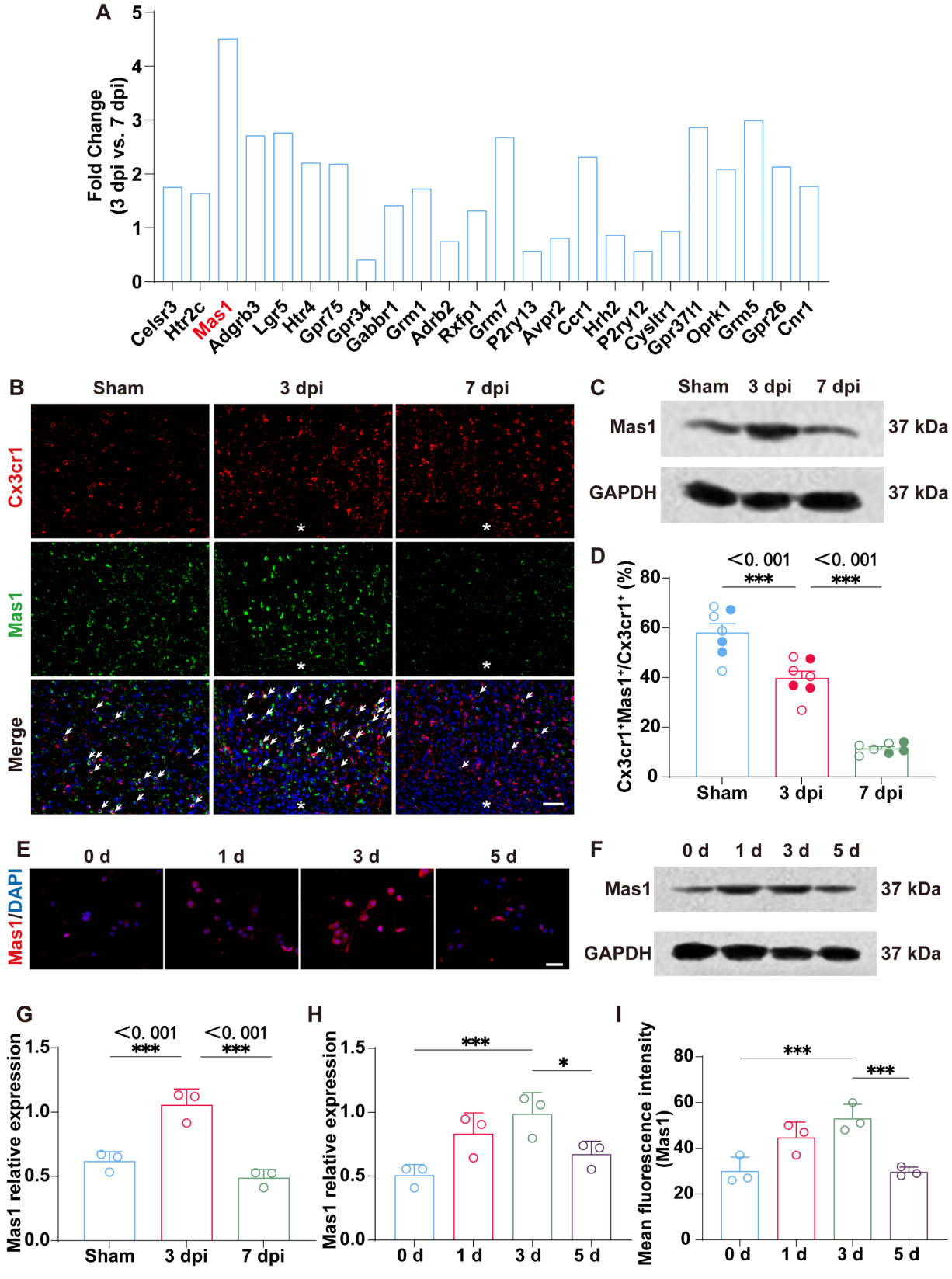

Fig. 6 (See legend on next page.)

(See figure on previous page.)

Fig. 6 Impaired microglial phagocytosis was accompanied by downregulation of Mas1 in vivo (**A**) Bar graph of the average expression levels of G protein-coupled receptor family members at 3 dpi and 7 dpi in macrophages/microglia after SCI transcriptomic data (GSE113566). (**B**) Representative immunofluorescence images of $Cx3cr1^+$ microglia (red), Mas1 (green) at 0–7 dpi in WT mice. The lesion core is marked with asterisks (*). (**C**) Western blot analysis of Mas1 at 0–7 dpi in WT mice. (**D**) Quantification of $Cx3cr1^+MBP^+$ microglia numbers at 0–7 dpi in WT mice. Hollow data points represent values from male mice. Solid data points denote female mice. (**E**) Representative immunofluorescence images of Mas1 in primary microglia incubated with myelin (1 mg/ml) at 0–5 d. (**F**) Western blot analysis of Mas1 in primary microglia incubated with myelin (1 mg/ml) at 0–5 d. (**G**) Quantification of Mas1 in primary microglia incubated with myelin (1 mg/ml) at 0–5 d (relative to GAPDH expression) in (**C**). (**H**) Quantification of Mas1 in primary microglia incubated with myelin (1 mg/ml) at 0–5 d (relative to GAPDH expression) in (**F**). (**I**) Quantification of MFI for Mas1 in primary microglia incubated with myelin (1 mg/ml) at 0–5 d in (**E**). Scale bar: 50 μm (**B**) and 20 μm (**E**). Data are presented as means ± SD. $n = 7$ mice per group in (**D**). $n = 3$ independent cultures in (**G**-**I**). $^{*}p < 0.05$, $^{**}p < 0.01$, $^{***}p < 0.001$ by oneway ANOVA followed by Tukey's post hoc test

60% of $Cx3cr1^+$ microglia in the uninjured spinal cord. Approximately 40% of $Cx3cr1^+$ microglia expressed Mas1 at 3 dpi, while this proportion declined to less than 15%, coinciding with microglial phagocytosis blockage at 7 dpi (Figs. 6B and 6D). Western blot results showed that the expression of Mas1 was upregulated at 3 dpi but downregulated significantly at 7 dpi (Figs. 6C and 6G). These results indicated a positive correlation between Mas1 levels and the phagocytic capacity of microglia. Furthermore, both immunofluorescence and western blot analyses confirmed that Mas1 expression was upregulated at 1 and 3 days but downregulated significantly at 5 days after myelin debris induction in vitro (Figs. 6E, 6F, 6H and 6I). The above results suggest that Mas1 may be a key upstream molecule regulating microglial phagocytosis after SCI.

To further confirm whether Mas1 mediates microglial phagocytosis through the PKC/Fascin-1 pathway, we employed the Mas1 agonist captopril to activate Mas1 and the PKCγ inhibitor BIM to inhibit the activation of the PKC/Fascin-1 pathway induced by Mas1 in vitro [27]. Immunofluorescence results showed that captopril significantly activated the Mas1/PKCγ pathway, promoted Fascin-1 phosphorylation, and enhanced microglial engulfment of myelin debris before and after 5 days of myelin debris induction (Figs. 7A-D and 7F). Importantly, compared with the captopril group, inhibition of PKCγ by BIM significantly hindered Fascin-1 phosphorylation and microglial phagocytosis (Fig. 7A-D and F). The quantitative analysis of western blot showed consistent results with the above immunocytochemistry data (Figs. 7E, 7G and 7H). In conclusion, these results indicate that Mas1 is an upstream molecule positively regulating the PKC/Fascin-1 pathway and mediating microglial phagocytosis.

Modulating Fascin-1 phosphorylation for neuroprotection and locomotor function recovery after SCI

To explore the therapeutic potential of targeting Fascin-1 phosphorylation post-SCI, we administered daily intraperitoneal injections of captopril in SCI mice to activate the PKCγ/Fascin-1 pathway, thereby modulating the balance of Fascin-1 phosphorylation in vivo. Immunofluorescence results showed that the number of $NeuN^+$ neurons in the Z1-Z4 region of injured spinal cord at 28 dpi was higher in mice received captopril treatment, as compared to the control group (Figs. 8A-C). LFB staining results indicated that a greater demyelinated lesion area in control mice than in captopril treated mice at 28 dpi (Supplemental Figs. 2C and 2D). Additionally, the mice in captopril group achieved better hindlimb locomotor function at 28 dpi, corresponding to higher BMS scores (Fig. 8D). Footprint analysis further showed that the captopril-treated mice had longer stride lengths, shorter stride widths and smaller paw rotation angles at 28 dpi, indicating improved locomotor function (Figs. 8E-H). In conclusion, these findings suggest that modulating the balance of Fascin-1 phosphorylation by activating the Mas1/PKCγ/Fascin-1 pathway is a potential strategy for SCI treatment (Fig. 9).

Discussion

Microglia play a pivotal role in promoting tissue repair by efficiently clearing myelin debris during the acute phase after SCI [4–6]. Our previous investigation identified a specific upregulation of Fascin-1 in microglia after SCI [8]. In this study, we utilized *Fascin-1* CKO mice subjected to a spinal cord crush injury model to elucidate the functional significance of Fascin-1 in microglial phagocytosis. Our findings underscore that Fascin-1 ablation in microglia exacerbates neuronal loss and impedes neurological recovery after SCI. We highlight that the actin-binding protein Fascin-1 in modulating microglial function, particularly by enhancing the phagocytosis of myelin debris in a time dependent manner, thus implicating Fascin-1 as indispensable for the generation of microglial responses to myelin debris. Mechanistically, our results reveal that the phagocytic activity of microglia is governed by the phosphorylation of Fascin-1, orchestrated downstream of the Mas1/PKCγ signaling axis. Notably, pharmacological intervention targeting the Mas1/PKCγ axis with captopril effectively restores the balance of Fascin-1 phosphorylation and microglial phagocytosis, consequently ameliorating neuronal loss and promoting neurological recovery after SCI. Collectively, our study elucidates a molecular mechanism involving dynamic Fascin-1 phosphorylation in the regulation of microglial phagocytosis.

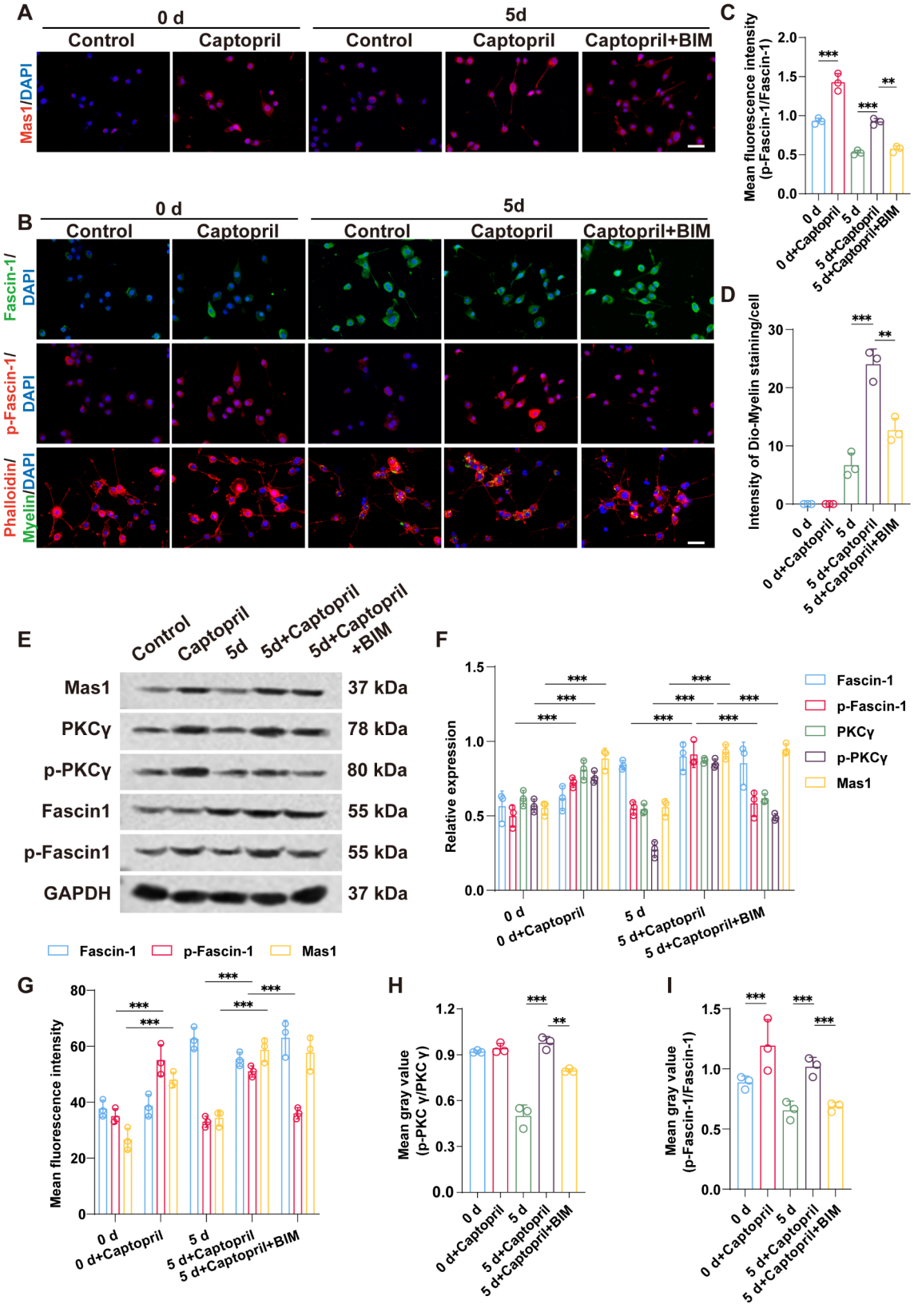

Fig. 7 (See legend on next page.)

(See figure on previous page.)

Fig. 7 Mas1 could be the upstream receptor to restore partial microglial phagocytosis in vitro (**A**) Representative immunofluorescence images of Mas1 (red) at 0 or 5 d in primary microglia incubated with myelin (1 mg/ml) treated with captopril (22 μg/ml, a Mas1 receptor agonist) or BIM (25 μg/ml, a inhibitor of PKCγ). (**B**) Representative immunofluorescence images of Fascin-1 (red), p-Fascin-1 (green) and primary microglia (phalloidin staining, red) incubated with Dio-myelin (1 mg/ml, green) at 0 or 5d in primary microglia incubated with myelin (1 mg/ml) treated with captopril (22 μg/ml, a Mas1 receptor agonist) or BIM (25 μg/ml, a inhibitor of PKCγ). (**C**) Quantification of p-Fascin-1/Fascin-1 in (**B**). (**D**) Quantification of intensity of Dio-Myelin staining/cell at 0 or 5 d in primary microglia with captopril or BIM treatment. (**E**) Western blot analysis of Mas1, PKCγ, p-PKCγ, Fascin-1 and p-Fascin-1 at 0 or 5 d in primary microglia with captopril or BIM treatment. (**F**) Quantification of MFI for Mas1, PKCγ, p-PKCγ, Fascin-1 and p-Fascin-1 at 0 or 5 d in primary microglia with captopril or BIM treatment in (**A**) and (**B**). (**G**) Quantification of Mas1, PKCγ, p-PKCγ, Fascin-1 and p-Fascin-1 at 0 or 5 d in primary microglia with captopril or BIM treatment (relative to GAPDH expression) in (**E**). (**H**) Quantification of p-PKCγ/PKCγ in (**E**). (**I**) Quantification of p-Fascin-1/Fascin-1 in (**E**). Scale bar: 20 μm (**A**) and (**B**). Data are presented as means ± SD. $n = 3$ independent cultures in (**C**), (**D**), (**F**), and (**G**-**I**). $^{*}p < 0.05$, $^{**}p < 0.01$, $^{***}p < 0.001$ by oneway ANOVA followed by Tukey's post hoc test

Axonal rupture and subsequent demyelination lead to the accumulation of abundant myelin debris within and around the injury core after SCI [28]. Myelin debris increases dramatically in the first week and persists in the spinal cord microenvironment for an extended period [4, 29]. Previous research has implicated the abnormal buildup of myelin debris in various detrimental effects, including the inhibition of axonal regeneration, suppression of oligodendrocyte maturation, induction of pro-inflammatory cytokine release, and exacerbation of macrophage infiltration [2, 3, 30, 31]. Microglia respond promptly to the presence of myelin debris within 24 h, engaging in direct interactions with damaged axons and emerging as the predominant phagocytic cell at 3 dpi [4]. Notably, microglia exhibit nearly five times the myelin debris engulfment rate compared to macrophages at 3 dpi. However, less than 5% of microglia contained myelin debris at 7 dpi. This mirrors the results from our study. Microglia exhibit robust phagocytic activity in the early injury stage without transforming into foamy cells. However, during the initial week post-injury, microglia appear to experience phagocytosis blockage. Subsequently, macrophages gradually replace microglia as the main phagocytic cells. Phagocytosis of myelin debris by foamy macrophages triggers the release of pro-inflammatory cytokines, exacerbating neuroinflammatory responses. Therefore, microglial phagocytosis of myelin debris is critical for SCI repair. Understanding the key regulatory mechanisms of microglial phagocytosis explored in this study would be beneficial to ameliorate microglial phagocytosis blockage, thereby alleviating local inflammation after injury and inhibiting the formation of foamy macrophages.

As a critical actin-binding protein, Fascin-1 regulates cell migration, invasion, and adhesion. Our previous studies indicated that Fascin-1 is predominantly expressed in microglia following SCI, with negligible expression in oligodendrocytes and macrophages [8]. Upon microglial activation, Fascin-1 expression was consistently upregulated but did not exhibit a significant association with microglial M1 pro-inflammatory and M2 anti-inflammatory phenotypes. Elevated levels of Fascin-1 facilitated microglial migration, contributing to scar formation around the injured region and enhancing recovery of motor function [32]. Our subsequent research confirmed that Fascin-1 limits myosin activity in microglia, thereby regulating the mechanical properties of the injured spinal cord. Given the role of microglial scar formation in facilitating tissue repair following SCI, coupled with the ability of Fascin-1 to promote microglial migration, we present novel evidence showing that specific deletion of Fascin-1 in microglia disrupts the spatial organization of $CD68^{+}$ microglia/macrophages at the injury site [10]. This disruption leads to a greater dispersion of microglia/macrophages across the lesion area rather than their aggregation at the injury core, highlighting a critical role of Fascin-1 in maintaining the localized accumulation of microglia/macrophages necessary for effective injury response and repair Despite low expression in macrophages and monocytes post-SCI, *Cx3cr1*^{cre} mice have been demonstrated as effective tools for genetic manipulation specifically in microglia [5, 33]. Leveraging this, we conducted the *Fascin-1 CKO* mice to investigate the function of Fascin-1 in microglia in this study. Our findings demonstrated that Fascin-1 deficiency in microglia dramatically exacerbated neuronal loss at the site of injury and impaired hind limb swing function, underscoring the beneficial role of microglial Fascin-1 in rapid response and pathology mitigation after SCI. Further investigation into microglial phagocytic capacity revealed that the absence of Fascin-1 in microglia inhibited the engulfment of myelin debris both in vivo and in vitro. These results collectively suggest that the protective function of microglia during the initial week post-SCI may be attributable to Fascin-1.

The role of Fascin-1 in maintaining actin polymerization and depolymerization hinges on the delicate balance of Fascin-1 phosphorylation. Notably, the Ser-39 residue within the Fascin-1 sequence serves as a pivotal phosphorylation site, where active PKCα or PKCγ directly engages with Ser-39 via the C1B domain of the PKC regulatory region [34]. Furthermore, the dynamic interplay between Fascin-1 and PKC is prominently observed within cellular protrusions and filopodia during cell migration, with the efficacy of these interactions contingent upon Fascin-1 phosphorylation status and

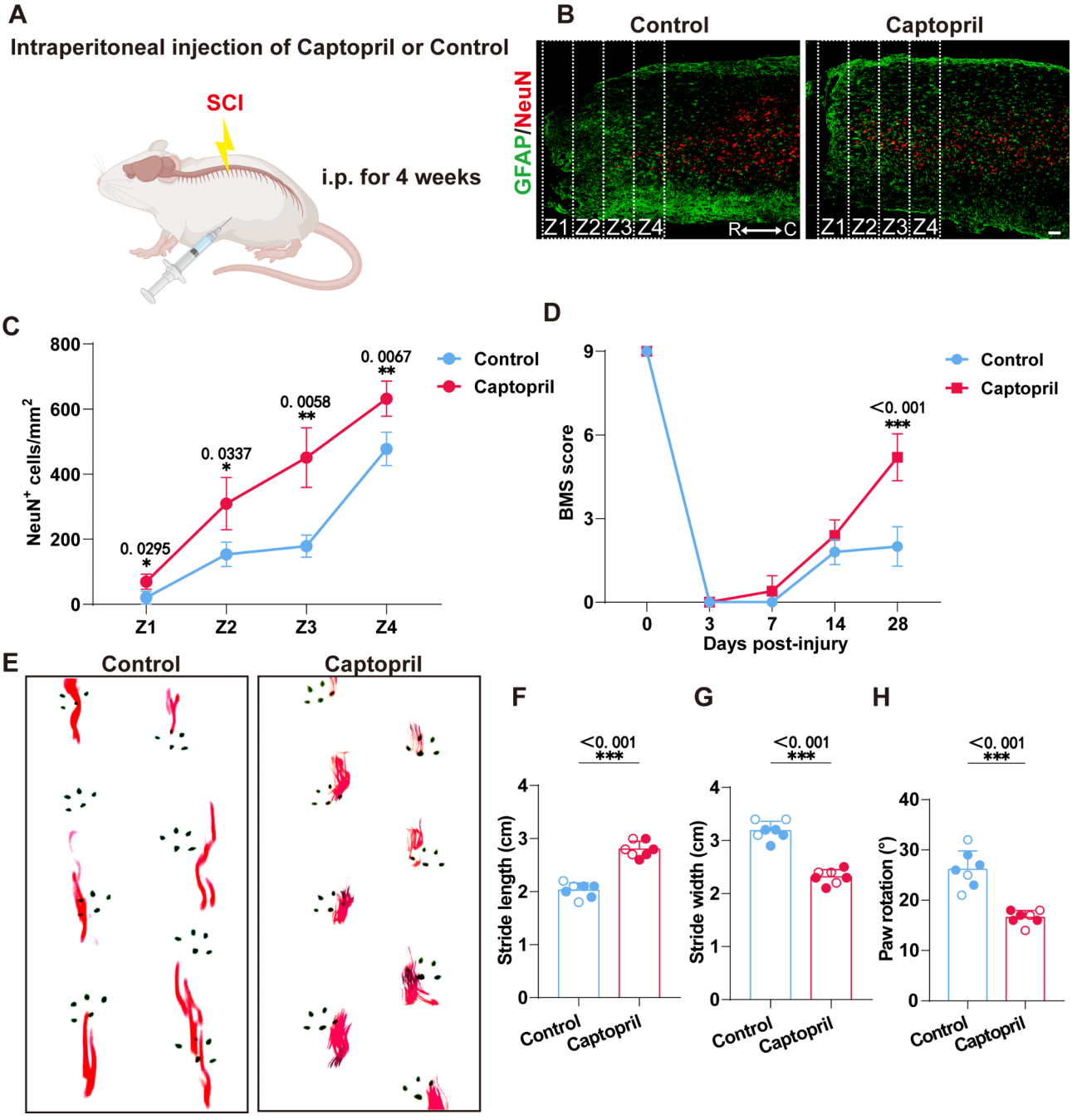

Fig. 8 Intraperitoneal injection of captopril protected residual neurons and promotes locomotor recovery after SCI (**A**) Mice were injected intraperitoneally with captopril (39 mg/kg) or the control solvent immediately after surgery until 28 dpi. (**B**) Representative immunofluorescence images of GFAP$^+$ astrocytes (green) and NeuN$^+$ neurons (red) in Z1-Z4 zones adjacent to the lesion core in mice treated with or without captopril (39 mg/kg) at 28 dpi. R and C represent the rostral and caudal sides of the injury respectively. (**C**) Quantification of NeuN$^+$ neurons numbers in (**B**). (**D**) Behavioral testing using the BMS score was performed at 0–28 dpi in mice treated with or without captopril (39 mg/kg). $^*p<0.05$, $^{**}p<0.01$, $^{***}p<0.001$ in (**C**) and (**D**) by twoway ANOVA followed by Tukey's post hoc test. (**E**) Footprint assays in mice treated with or without captopril (39 mg/kg) at 28 dpi. (**F**-**H**) Quantification of Paw rotation (**F**) Stride length (**G**) Stride width (**H**) in Footprint assays. Hollow data points represent values from male mice. Solid data points denote female mice. Scale bars: 100 μm (**B**). Data are presented as means ± SD. $n=7$ mice per group in (**C**-**H**). $^*p<0.05$, $^{**}p<0.01$, $^{***}p<0.001$ in (**F**-**H**) by Student's t test

PKC activity [23]. Sema5A induces PKC phosphorylation of fascin-1, thereby reducing its actin-binding/bundling activity to inhibit cell migration and invasion in human gliomas [13]. Remarkably, pharmacological inhibition of PKC activity with BIM leads to notable alterations in cellular morphology, characterized by shortened and rigid filopodia, concomitant with enhanced cell migration [23]. These effects are accompanied by a discernible

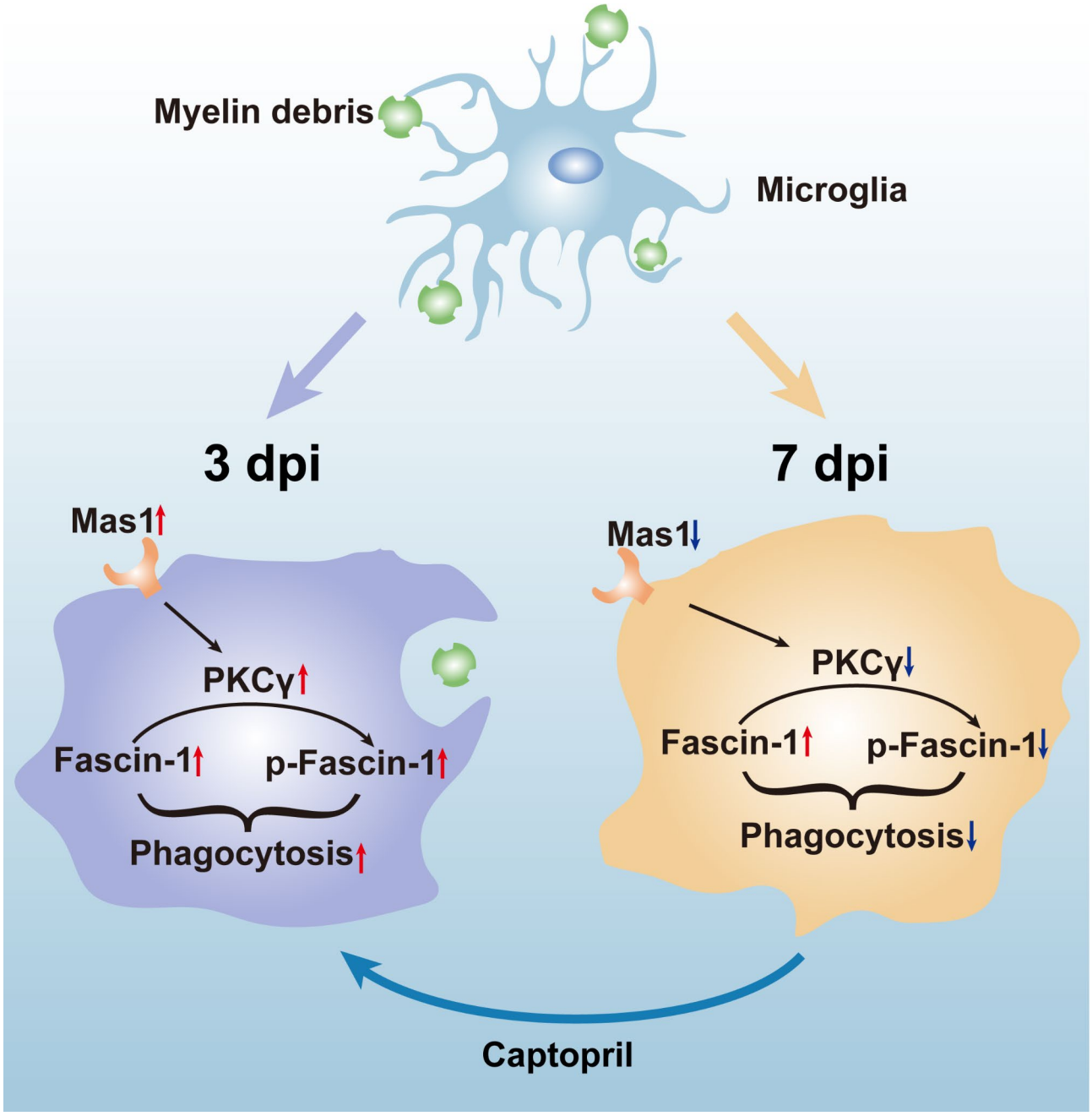

Fig. 9 The function of the balance of Fascin-1 phosphorylation in modulating microglial phagocytosis following SCI. Microglia has extremely robust phagocytic activity in early injury stage (3 dpi), but appears phagocytosis blockage in subacute stage (7 dpi). Pharmacological intervention targeting the Mas1/PKCγ axis with captopril effectively restores the balance of Fascin-1 phosphorylation and microglial phagocytosis

modulation of the balance of Fascin-1 phosphorylation, underscoring the regulatory significance of Fascin-1 phosphorylation in governing cellular dynamics. In this study, we found that the phosphorylation level of Fascin-1 gradually decreased during the first week after SCI, hinting at a potential correlation between the diminished phagocytic capacity of microglial cells and the perturbation in Fascin-1 phosphorylation. Notably, we unveiled concomitant alterations in PKCγ levels at both transcriptional and protein levels, suggesting a coordinated regulation with Fascin-1 phosphorylation dynamics. Importantly, activating PKCγ using TPA in primary microglia promoted Fascin-1 phosphorylation and enhanced microglial phagocytosis. This implicates PKCγ as a pivotal kinase orchestrating Fascin-1 phosphorylation in microglial phagocytosis. We are further exploring more pharmacological agents that might influence Fascin-1 phosphorylation in our study. Future research

should concentrate on elucidating the molecular mechanisms underlying Fascin-1 phosphorylation by specifically targeting the phosphorylation site of Fascin-1 and examining the protein expression of PKCγ.

The surface of microglia is rich in G protein-coupled receptors, which assist in recognizing cellular debris and initiating the phagocytic process, thereby expediting clearance and neuroprotection [35, 36]. G protein-coupled receptors represent classical upstream receptors that regulate PKC function [37]. In this study, we analyzed transcriptomic data of microglia/macrophages after SCI and found that Mas1 was the G protein-coupled receptor with the most significant expression level changes between 3 and 7 dpi. Further investigation of Mas1 expression after SCI and in vitro microglial phagocytosis model revealed that a correlation with microglial phagocytic ability. In our in vitro model, activation of Mas1 combined with inhibition of PKCγ revealed that the Mas1/PKCγ axis regulated Fascin-1 phosphorylation, thereby promoting microglial phagocytosis. This underscores Mas1 as a pivotal regulator in promoting microglial Fascin-1 phosphorylation to augment phagocytic activity. Captopril, an agonist of Mas1, has been used in the treatment of neurological and psychiatric disorders [38]. In the murine lupus model, intraperitoneal administration of Captopril reduced hippocampal and cerebral cortex levels of C3 and IgG, ameliorating intracerebral inflammation [39]. Our findings underscore the potential of Captopril in salvaging Fascin-1 phosphorylation in microglia, thereby safeguarding residual neurons and fostering locomotor recuperation. It should be acknowledged that Mas1 is not solely expressed in $Cx3cr1^{+}$ microglia, implying potential involvement of other cell types. Notably, the influence on the regulation of vascular endothelial cells and revascularization in the spinal cord microenvironment might be a significant contributor to the recovery of motor function in mice after SCI. Consequently, the beneficial effects of captopril on spinal cord injury (SCI) extend beyond its impact on Fascin-1 phosphorylation and the intricate molecular processes involved warrant extensive exploration. Further inquiries are warranted to delineate the cellular distribution of Mas1 and ascertain the most efficacious administration route. These endeavors will provide crucial insights into the precise mechanisms underpinning the therapeutic effects of Captopril and optimize its clinical translation for SCI treatment.

In summary, our study elucidates the pivotal role of Fascin-1 phosphorylation in governing microglial phagocytosis after SCI, confirming the significance of the Mas1/PKCγ axis in modulating this phosphorylation balance. Targeting the activation of the Mas1/PKCγ axis emerges as a promising therapeutic strategy for preserving residual neurons and fostering locomotor function recovery following SCI. These findings shed light on potential avenues for SCI intervention, emphasizing the importance of precise molecular regulation in maintaining the balance of Fascin-1 phosphorylation to promote neuroprotection and functional restoration.

Limitations of the study part

In this study, the $Cx3cr1^{cre+/-}$ mouse line was used to achieve microglia-specific knockdown of Fascin-1. In addition to microglia, this mouse line also affects perivascular and blood-derived macrophages which express Cx3cr1 [40]. $Cx3cr1^{cre+/-}$ mice have a minimal probability of leakage into neurons [41]. Our investigation concentrated on microglial phagocytosis during in vivo experiments conducted from 1 to 7 dpi, as prior studies have indicated that macrophages are not yet the predominant phagocytic cells within the microenvironment during this time window [4]. Our previous studies have shown that the proportion of cells other than microglia expressing Fascin-1 is exceptionally low, which partly supports the reliability of our model [8]. Therefore, $Cx3cr1^{cre}$ mice remain a crucial tool for the specific targeting of microglial cells. In the context of microglial phagocytosis, Cx3cr1 has been widely recognized in previous studies as a key microglial marker. Cx3cr1 functions as a receptor that significantly influences phagocytic activity. It plays an integral role in the communication between microglia and neurons, with its signaling pathways modulating the microglial response to injury and disease. By regulating the recruitment and activation of microglia, Cx3cr1 impacts their ability to engulf and clear cellular debris, pathogens, and other harmful substances within the CNS [42, 43]. The genotype of the transgenic mice used in our research was $Cx3cr1^{cre+/-}$;$Fascin\text{-}1^{fl/fl}$, with a partial knockout of Cx3cr1, which may result in partially impaired microglial phagocytosis. Controls including $Cx3cr1^{cre+/-}$ and $Fascin\text{-}1^{fl/fl}$ are provided in Supplementary Fig. 3 and the results indicate that Fascin-1 ablation is critical for the impairment of microglial phagocytosis. However, we cannot entirely exclude the possibility that Cx3cr1 deletion may have an interfering or synergistic effect on Fascin-1 deficiency. Therefore, it is important to acknowledge the limitations associated with the use of $Cx3cr1^{cre+/-}$ mice in this study. Further research is necessary to establish *Tmem119* [2] or $Hexb^{cre}$ mouse line that would allow for the specific elimination of Fascin-1 in microglia.

Supplementary Information

The online version contains supplementary material available at https://doi.org/10.1186/s12974-025-03445-z.

Supplementary Material 1

Supplementary Material 2

Acknowledgements
This project has received funding from the National Natural Science Foundation of China (Grant Nos. 82271413 and 82372506), the Clinical Medicine Translational Research Special Projects of Anhui Province (Grant Nos. 202304295107020009, 202304295107020013 and 202304295107020014), the Natural Science Foundation of Anhui Province (Grant Nos. 2208085MH222, 2308085MH257 and 2308085QH266), and the Natural Science Research Key Project of Colleges and Universities of Anhui Province (Grant Nos. KJ2021A0310, 2022AH050650, 2022AH050746, and 2022AH050713), Research Fund of Anhui Medical University (Grant No. 2023xkj031), the National Funded Postdoctoral Researcher Program of China (Grant Nos. GZC20230027), Anhui Postdoctoral Scientific Research Program Foundation (Grant No. 2024C880), and the Natural Science Foundation Incubation Program of The Second Affiliated Hospital of Anhui Medical University (Grant Nos. 2022GQFY04 and 2024GQFY05). We are grateful to the Scientific Research and Experiment Center of the Second Affiliated Hospital of Anhui Medical University.

Author contributions
J.H.J, L.C, and M.G.Z designed the research. Y.C.L, F.Y, and Z.Y.L performed the experiments. J.J.L, Y.J and X.Y.H analyzed the data. Y.C.L, F.Y, and Z.Y.L wrote the manuscript. J.H.J, L.C, M.G.Z, S.S.Y, and F.Y.O.Y reviewed and edited the manuscript.

Data availability
The data will be made available upon reasonable request to the corresponding authors.

Declarations

Competing interests
The authors declare no competing interests.

Received: 24 October 2024 / Accepted: 13 April 2025
Published online: 25 April 2025

References

1. Timothy JK, John CG. Myelin as an inflammatory mediator: Myelin interactions with complement, macrophages, and microglia in spinal cord injury. J Neurosci Res. 2018;96(6):969–77. https://doi.org/10.1002/jnr.24114.
2. Tian Z, Yiming Z, Li S, Smaranda Ruxandra B, Yuanhu J, Yang L, et al. Microvascular endothelial cells engulf Myelin debris and promote macrophage recruitment and fibrosis after neural injury. Nat Neurosci. 2019;22(3):421–35. https://doi.org/10.1038/s41593-018-0324-9.
3. Marie TF. Myelin-associated inhibitors of axonal regeneration in the adult mammalian CNS. Nat Rev Neurosci. 2003;4(9):703–13. https://doi.org/10.1038/nrn1195.
4. Andrew DG, Samuel D. Differences in the phagocytic response of microglia and peripheral macrophages after spinal cord injury and its effects on cell death. J Neurosci Res. 2014;34(18):6316–22. https://doi.org/10.1523/jneurosci.4912-13.2014.
5. Victor B-L, Floriane B, Benoit M, Nicolas V, Martine L, Marie-Eve J, et al. Microglia are an essential component of the neuroprotective Scar that forms after spinal cord injury. Nat Commun. 2019;10(1):518–32. https://doi.org/10.1038/s41467-019-08446-0.
6. Faith HB, Yang L, Cankun W, Anjun M, Qi G, Yi L, et al. Microglia coordinate cellular interactions during spinal cord repair in mice. Nat Commun. 2022;13(1):4096–108. https://doi.org/10.1038/s41467-022-31797-0.
7. Zhu Y, Lyapichev K, Lee DH, Motti D, Ferraro NM, Zhang Y, et al. Macrophage transcriptional profile identifies lipid catabolic pathways that can be therapeutically targeted after spinal cord injury. J Neurosci. 2017;37(9):2362–76. https://doi.org/10.1523/jneurosci.2751-16.2017.
8. Shuisheng Y, Li C, Dasheng T, Ziyu L, Fei Y, Yang L, et al. Fascin-1 is highly expressed specifically in microglia after spinal cord injury and regulates microglial migration. Front Pharmacol. 2021;12(0):729524. https://doi.org/10.3389/fphar.2021.729524.
9. Josephine CA. Roles of fascin in cell adhesion and motility. Cell Biol. 2004;16(5):590–6. https://doi.org/10.1016/j.ceb.2004.07.009.
10. Jinxin H, Xuyang H, Zeqiang C, Fangru O, Jianjian L, Yixue H, et al. Fascin-1 limits myosin activity in microglia to control mechanical characterization of the injured spinal cord. J Neuroinflammation. 2024;21(1):88–104. https://doi.org/10.1186/s12974-024-03089-5.
11. Tetsuhisa O, Yosuke O, Kazuyo M, Takuya M, Akiyo K, Shigenobu Y, et al. IKKε inhibits PKC to promote Fascin-dependent actin bundling. Development. 2016;143(20):3806–16. https://doi.org/10.1242/dev.138495.
12. Martina S, Sangeetha G, Maddy P, Yafeng M, Carl H, Marc PZ, et al. Fascin regulates the migration of subventricular zone-derived neuroblasts in the postnatal brain. J Neurosci Res. 2013;33(30):12171–85. https://doi.org/10.1523/jneurosci.0653-13.2013.
13. Li X, Law JWS, Lee AYW. Semaphorin 5A and plexin-B3 regulate human glioma cell motility and morphology through Rac1 and the actin cytoskeleton. Oncogene. 2011;31(5):595–610. https://doi.org/10.1038/onc.2011.256.
14. Sivakami M, Spencer AF, Sergio G. The cytoskeleton in phagocytosis and macropinocytosis. Curr Biol. 2021;31(10):619–32. https://doi.org/10.1016/j.cub.2021.01.036.
15. Ziyu L, Shuisheng Y, Yanchang L, Xuyang H, Yiteng L, Zhaoming X, et al. SU16f inhibits fibrotic Scar formation and facilitates axon regeneration and locomotor function recovery after spinal cord injury by blocking the PDGFRβ pathway. J Neuroinflammation. 2022;19(1). https://doi.org/10.1186/s12974-12022-02449-12973https://doi.org/10.1186/s12974-022-02449-3. IF: 9.3 Q1 B1
16. Fei Y, Yang L, Yanchang L, Yihao C, Yiteng L, Xuyang H, et al. Imatinib inhibits pericyte-fibroblast transition and inflammation and promotes axon regeneration by blocking the PDGF-BB/PDGFRβ pathway in spinal cord injury. Inflamm Regen. 2022;42(1):44–56. https://doi.org/10.1186/s41232-022-00223-9.
17. Siling D, Shanshan X, Xiangjuan D, Ti-Fei Y, Bo P, Yanxia R. Primary microglia isolation from postnatal mouse brains. J Vis Exp. 2021;168e62237. https://doi.org/10.3791/62237.
18. Shuisheng Y, Ziyu L, Xinzhong X, Fei Y, Yang L, Yanchang L, et al. M1-type microglia can induce astrocytes to deposit chondroitin sulfate proteoglycan after spinal cord injury. Neural Regen Res. 2021;17(5):1072–9. https://doi.org/10.4103/1673-5374.324858.
19. Wei L, Xuhui G, Zheng Z, Dongdong J, Yuluo R, Jiaxing W, et al. Deubiquitinase USP18 regulates reactive astrogliosis by stabilizing SOX9. J Glia. 2021;69(7):1782–98. https://doi.org/10.1002/glia.23992.
20. Ina BW, Mark AA, Bingbing S, Jaclynn L, Ana F, Zachary G-T, et al. Glial Scar borders are formed by newly proliferated, elongated astrocytes that interact to corral inflammatory and fibrotic cells via STAT3-dependent mechanisms after spinal cord injury. J Neurosci. 2013;33(31):12870–86. https://doi.org/10.1523/jneurosci.2121-13.2013.
21. Masamitsu H, Kazu K, Yasuyuki O, Hiromi K, Kazuya Y, Takeyuki S, et al. Interaction of reactive astrocytes with type I collagen induces astrocytic Scar formation through the integrin-N-cadherin pathway after spinal cord injury. Nat Med. 2017;23(7):818–28. https://doi.org/10.1038/nm.4354.
22. Payam D, Fabien N, Heinz S, Anja S, Johannes H, Eike DS, et al. NO mediates microglial response to acute spinal cord injury under ATP control in vivo. Glia. 2010;58(9):1133–44. https://doi.org/10.1002/glia.20993.
23. Asier J, Maddy P, Josephine CA. A novel Rho-dependent pathway that drives interaction of fascin-1 with p-Lin-11/Isl-1/Mec-3 kinase (LIMK) 1/2 to promote fascin-1/actin binding and filopodia stability. BMC Biol. 2012;10(0):72–81. https://doi.org/10.1186/1741-7007-10-72.
24. Xiang Z, Shalaka W, Marie-Sophie F, Michael K, Caroline CF, Kleopatra A, et al. Microglia and macrophages promote corralling, wound compaction and recovery after spinal cord injury via Plexin-B2. Nat Neurosci. 2020;23(3):337–50. https://doi.org/10.1038/s41593-020-0597-7.
25. Davide C, Zsombor K, Yann L, Tamara M, Shannon OB. G protein-coupled receptor-G protein interactions: a single-molecule perspective. Physiol Rev. 2020;101(3):857–906. https://doi.org/10.1152/physrev.00021.2020.
26. Fabio C, Germano G, Melania P, Marta DM, Domenico T, Mariapia C, et al. Cell-surface receptors transactivation mediated by g protein-coupled receptors. Int J Mol Sci. 2014;15(11):19700–28. https://doi.org/10.3390/ijms151119700.
27. Mengxing T, Xiao X, Li G, Junling L, Junshan Z, Teng J, et al. Involvement of angiotensin-(1–7) in the neuroprotection of Captopril against focal cerebral ischemia. Neurosci Lett. 2018;687(0):16–21. https://doi.org/10.1016/j.neulet.2018.09.024.
28. Melanie DS, Zhen Z, Axel M, Amy RN, Berislav VZ. Blood-Brain barrier: from physiology to disease and back. Physiol Rev. 2018;99(1):21–78. https://doi.org/10.1152/physrev.00050.2017.
29. Christine BR, James SC, Hassan A-A, Jae KL. Myelin and non-myelin debris contribute to foamy macrophage formation after spinal cord injury. Neurobiol Dis. 2022;163(0):105608. https://doi.org/10.1016/j.nbd.2021.105608.

30. Mark RK, Wen-Wu L, Chao Z, Robin JMF. Myelin impairs CNS remyelination by inhibiting oligodendrocyte precursor cell differentiation. J Neurosci. 2006;26(1):328–32. https://doi.org/10.1523/jneurosci.2615-05.2006.
31. Sae-Bom J, Hee Jung Y, Se-Ho P, In-Hoo K, Eun Jung P. Sulfatide, a major lipid component of Myelin sheath, activates inflammatory responses as an endogenous stimulator in brain-resident immune cells. J Immunol. 2008;181(11):8077–87. https://doi.org/10.4049/jimmunol.181.11.8077.
32. Xuyang H, Jinxin H, Yiteng L, Lei D, Yihao C, Fangru O, et al. TAZ induces migration of microglia and promotes neurological recovery after spinal cord injury. J Front Pharmacol. 2022;13(0):983416. https://doi.org/10.3389/fphar.2022.938416.
33. Yi L, Xuelian H, Riki K, Yu Z, Qing W, Aboozar M, et al. Microglia-organized scar-free spinal cord repair in neonatal mice. Nature. 2020;587(7835):613–8. https://doi.org/10.1038/s41586-020-2795-6.
34. Maddy P, Josephine CA. Rac regulates the interaction of fascin with protein kinase C in cell migration. J Cell Sci. 2008;121(0):2805–13. https://doi.org/10.1242/jcs.022509.
35. Sonja K, Stine K, Marcin N, Urszula G, Ria W, Alexander B, et al. The G protein-coupled receptor 55 ligand l-α-lysophosphatidylinositol exerts microglia-dependent neuroprotection after excitotoxic lesion. Glia. 2013;61(11):1822–31. https://doi.org/10.1002/glia.22560.
36. Rouven S, Medina K-D, Alessandro V, Gloria C, Sandra S. Chimeric GPCRs mimic distinct signaling pathways and modulate microglia responses. Nat Commun. 2022;13(1):4728–39. https://doi.org/10.1038/s41467-022-32390-1.
37. Dehua Y, Qingtong Z, Viktorija L, Shanshan Q, Sanaz D, Yiran W, et al. G protein-coupled receptors: structure- and function-based drug discovery. Signal Transduct Target Ther. 2021;6(1):7–16. https://doi.org/10.1038/s41392-020-00435-w.
38. Han L, Pengfei W, Yu C, Ming J, Tiantian S, Ji W, et al. Angiotensin-Converting enzyme inhibitor rapidly ameliorates Depressive-Type behaviors via Bradykinin-Dependent activation of mammalian target of Rapamycin complex 1. Biol Psychiatry. 2020;88(5):415–25. https://doi.org/10.1016/j.biopsych.2020.02.005.
39. Xinyan D, Jianchen F, Donghui L, Xuehui W, Haoyu K, Lifen G, et al. Captopril alleviates epilepsy and cognitive impairment by Attenuation of C3-mediated inflammation and synaptic phagocytosis. J Neuroinflammation. 2022;19(1):226–40. https://doi.org/10.1186/s12974-022-02587-8.
40. Jung S, Aliberti J, Graemmel P, Sunshine M, Kreutzberg G, Sher A, et al. Analysis of fractalkine receptor CX(3)CR1 function by targeted deletion and green fluorescent protein reporter gene insertion. J Mol Cell Biol. 2000;20(11):4106–14. https://doi.org/10.1128/mcb.20.11.4106-4114.2000.
41. Xiaofeng Z, Mahabub Maraj A, Yuan L, Tingting H, Ramkumar M, Xinjun Z, et al. Targeting microglia using Cx3cr1-Cre lines: revisiting the specificity. J eNeuro. 2019;6(4):1–11. https://doi.org/10.1523/eneuro.0114-19.2019.
42. Matthew KZ, Lian Z, Yikui Z, Shaimar RG, Wenxin M, Xu W, et al. Microglial phagocytosis and activation underlying photoreceptor degeneration is regulated by CX3CL1-CX3CR1 signaling in a mouse model of retinitis pigmentosa. J Glia. 2016;64(9):1479–91. https://doi.org/10.1002/glia.23016.
43. Genaro EO, Maryanne NB, Robert AH. Microglial phagocytosis of single dying oligodendrocytes is mediated by CX3CR1 but not MERTK. J Cell Rep. 2024;43(7):114385. https://doi.org/10.1016/j.celrep.2024.114385.

Publisher's note